6th International Conference on Advances in Experimental Structural Engineering
11th International Workshop on Advanced Smart Materials and Smart Structures Technology
August 1-2, 2015, University of Illinois, Urbana-Champaign, United States

Effect of Steel Core Bending on the Seismic Performance of Buckling-Restrained Braces Using Steel-and-Mortar Planks for Buckling-Restraining System

Mitsumasa Midorikawa[1], Mamoru Iwata[2], Shunsuke Hishida[3]

Taichiro Okazaki[4], Tetsuhiro Asari[5]

1 *Professor, Dept. of Architectural and Structural Design, Hokkaido University, Japan, Dr. Eng.*
E-mail: midorim@eng.hokudai.ac.jp
2 *Professor, Dept. of Architecture and Building Eng., Kanagawa University, Japan, Dr. Eng.*
E-mail: iwata@kanagawa-u.ac.jp
3 *Graduate student, Dept. of Architectural and Structural Design, Hokkaido University, Japan, B. Eng.*
E-mail: sh_dia.-hishida-r.field_ke.o7l6@frontier.hokudai.ac.jp
4 *Associate Professor, Dept. of Architectural and Structural Design, Hokkaido University, Japan, Ph.D..*
E-mail: tokazaki@eng.hokudai.ac.jp
5 *Assistant Professor, Dept. of Architectural and Structural Design, Hokkaido University, Japan, Dr.Eng.*
E-mail: asari@eng.hokudai.ac.jp

ABSTRACT
Installation of buckling-restrained braces (BRBs) is an effective means to improve the seismic performance of building structures. The authors have developed a new variation of BRBs that use steel-and-mortar planks for the buckling-restraining system. A large number of laboratory test results, by the authors, suggest that BRBs using steel-and-mortar planks exhibit excellent performance on par with widely used commercialized BRB products. An experimental study was conducted, using the new BRBs, to examine how major-axis (out-of-plane) bending deformation of the steel core affects the cyclic loading performance. Four BRB specimens were fabricated in the laboratory. All specimens combined a flat-plate steel core with a relatively small width-to-thickness ratio of six, and a very stiff buckling-restraining system whose Euler buckling load was six times the yield strength of the steel core. Two specimens placed longitudinal round bars in the mortar-free gaps adjacent to the side of steel core. Two specimens kept the gaps empty by intension. The test results suggest that placement of round bars in the mortar-free gaps is an effective method to control major-axis bending deformation of the steel core. On the other hand, interestingly, the specimens that controlled major-axis bending deformation did not achieve better seismic performance than the specimens that allowed major-axis bending deformation.

KEYWORDS: Buckling-restrained braces, Cyclic loading test, Compressive-to-tensile strength ratio, Buckling-mode number, Slenderness ratio, Friction force

1. INTRODUCTION

Installation of buckling-restrained braces (BRBs) is an effective means to improve the seismic performance of existing buildings. Performance enhancement is possible to the extent that, during a severe earthquake, plastic deformation is concentrated in the BRBs while all other structural elements remain elastic. The authors have developed a new variation of BRBs that use steel-and-mortar planks for the buckling-restraining system. These new BRBs allow for are easy manufacturing and easy quality control. Furthermore, unlike most commercialized products, the configuration and size of the bracing connection is not limited by the buckling-restraining system. A large number of laboratory tests by Iwata & Murai (2006) suggest that BRBs using steel-and-mortar planks exhibit excellent performance on par with widely used commercialized BRB products. However, it was also recognized that the steel core of these BRBs develop bending deformation about the major axis [Hishida et al. (2015)]. Major-axis bending deformation (out-of-plane deformation) of the BRB should be controlled out of concern that such deformation can cause damage to surrounding members. On the other hand, Midorikawa et al. (2014a, 2014b) report that the compressive strength of BRBs tends to increase with buckling-mode number of the steel core about the minor axis. In view of these circumstances, four BRB specimens were tested to examine how to effectively control major-axis bending deformation of the steel core and how deformation (about the minor axis and major axis) of the steel core can affect the seismic performance of BRBs.

2. TEST PROGRAM

2.1. Test specimens

Figure 2.1 and Figure 2.2 show four, full-scale specimens constructed for this project. All specimens used a 72 mm-by-12 mm plate for the steel core. In this paper, the major and minor axes refer to the two primary bending axes associated with the cross section of the steel core. The steel core was wrapped by unbonding material, 1.0-mm thick butyl rubber, to create a clearance for minor-axis bending deformation, C_w, between the steel core and the mortar. A clearance for major-axis bending deformation, C_s, was also created between the side of steel core and round bar, or, in the absence of a round bar, between the steel core and steel channel. A shear key was welded at each side of the steel core in the middle of the yielding segment. The function of the shear key is to prevent slipping of the buckling-restraining system relative to the steel core.

Table 2.1 lists key properties of test specimens. Specimen N-C02RS represented a standard BRB except for the grooves in the mortar to facilitate research objectives. Table 2.2 lists material properties established from tension coupon tests. The steel core used SN400B steel, and the buckling-restraining system used either SS400 or WEL-TEN 590RE steel. SN is a structural steel with a specified yield-to-tensile strength ratio. SS is a standard structural steel. WEL-TEN is a high-strength steel with good weldability used in machines. The slenderness ratios of the steel core, λ_w and λ_s, computed as the length of the yielding segment, L = 1,251 mm, divided by the radius of gyration about the minor or major axis, were 360 and 60, respectively. The ratio P_E/P_y, where P_E is the Euler load of the buckling-restraining system and P_y is the yield strength of the steel core is commonly used to evaluate whether the buckling-restraining system is sufficiently stiff to prevent overall buckling of the steel core. The ratio is also used as a parameter to estimate the energy dissipation capacity of BRBs. The specimens were provided with a rather high ratio of P_E/P_y = 6, while BRBs are typically designed

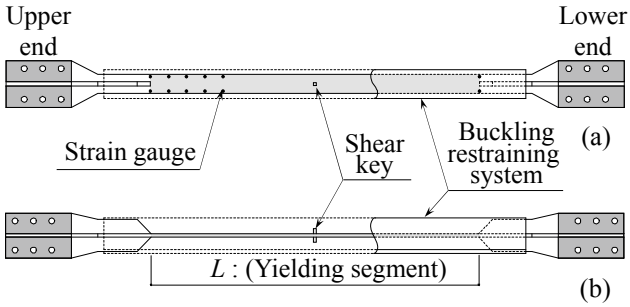

Figure 2.1 Top view and side view of specimens : (a) Top view ; (b) Side view

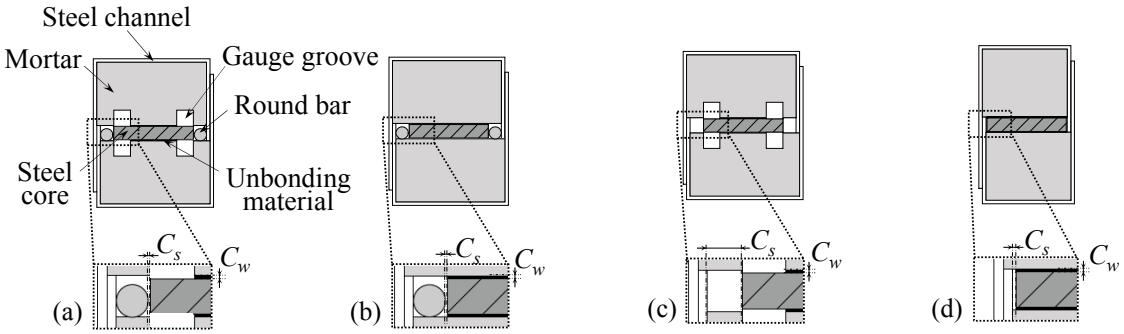

Figure 2.2 Cross section of specimens : (a) N-C02RS ; (b) H-C02R ; (c) N-C24S ; (d) N-C02

Table 2.1 List of test specimens

Specimen	Steel core				Buckling restraining system						
	λ_w	λ_s	L (mm)	P_y (kN)	Steel grade	Cross section (mm)	P_E (kN)	P_E/P_y	C_w (mm)	C_s (mm)	Round bar
N-C02RS	360	60	1251	283	SS400	C-105.6×74.5×121×3.2	1930	6	1	1	Yes
H-C02R					WEL-TEN590RE						Yes
N-C24S					SS400					12	No
N-C02						C-83.6×79×130×3.2	1938			1	No

Note) Steel core : Cross section = PL-72 × 12, Width-to-thickness ratio = 6

Table 2.2 Mechanical properties of steel core, steel channel and mortar

(a) Steel core and steel channel

Steel grade	Thickness (mm)	Yield stress (N/mm^2)	Tensile strength (N/mm^2)	Yield ratio (%)	Yield strain (%)
SN400B	12	328	449	73.1	0.174
SS400	3.2	292	446	65.4	0.171
WEL-TEN590RE		597	682	87.4	0.435

(b) Mortar

Specimen	Compressive strength N/mm^2
N-C02RS H-C02R	73.2
N-C24S N-C02	64.6

for P_E/P_y = 3.0 to 4.5. The two specimens including an 'R' in their identification placed a round bar next to each edge of the steel core to fill the gap between the steel core and channel. The two specimens whose identification ends with an 'S' were prepared with a dense array of strain gauges on the surface of the steel core. As indicated in Figure 2.2, longitudinal grooves were produced in the mortar to allow the lead wires to extend outside of the buckling-restraining system. Previous tests have proven that the placement of strain gauges and the groove in mortar does not affect the cyclic loading performance of the BRB [Midorikawa et al. (2012)]

2.2. Test setup, loading protocol and measurement

Figure 2.3 illustrates the test setup that loaded BRB specimens in a 45° orientation. Static loading was applied by controlling the axial strain, ε, of the yielding segment of the steel core, evaluated as the relative displacement between points A and B in the figure, divided by the length of the yielding segment. The loading protocol is shown in Table 2.3. The final amplitude of 3.0% was continued until the strength decreased to 80% of the maximum measured strength.

3. TEST RESULTS AND DISCUSSION

3.1. Progress and final state of specimens

Figure 3.1 shows the relationship between the normalized axial force, P/P_y, where P is the axial load, and axial strain, ε, for each specimen. All specimens exhibited stable hysteresis up to a high strain amplitude of 3.0%. However, specimen N-C24S exhibited a strength reduction and recovery during compression loading starting strain amplitude 1.0%. This phenomena was not seen in the other three specimens. Figures 3.2a and b show bulging of the steel channel observed in specimens N-C24S and N-C02 that started during strain amplitude 1.5%. Figures 3.2c and d show bulging in specimens N-C02RS and N-C24S, on the top and bottom sides of the steel channel, at the end of the test.

It appeared that the steel core bent about its major axis and started to bear against the steel channel. The deformation of steel channel was not observed in the other two specimens. The strength decrease and recovery in compression observed in specimen N-C24S was likely associated with this deformation. It is postulated that once the steel core contacted the channel, the channel restrained further deformation, and thereby allowed some recovery in strength. While deformation of the channel was also observed in specimen N-C02, this specimen did

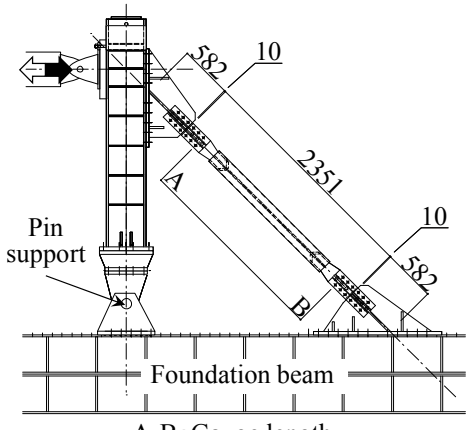

A-B : Gauge length

Figure 2.3 Test setup (Unit : mm)

Table 2.3 Loading protocol

Strain amplitude (%)	Number of cycles
$\varepsilon_y/3$	1
$2\varepsilon_y/3$	1
0.25	1
0.5	2
0.75	2
1.0	5
1.5	2
2.0	2
2.5	2
3.0	---

not show the decrease and recovery seen in specimen N-C24S. Consequently, it appeared that major-axis bending of the steel core affected the cyclic loading performance of specimen N-C24S but did not affect the other three specimens. Specimens N-C02RS and N-C24S decreased on strain amplitude 3.0%. Consequently, it appeared that minor-bending deformation of steel channel was observed at the end of the test

Table 3.1 lists the last half cycle when failure occurred, i.e., the strain amplitude when the strength at peak amplitude reduced to below 80% of the maximum measured strength, and the failure mode identified after the test was completed. All four specimens failed due to tensile fracture of the steel core. The fracture occurred in the yielding segment either near the core projection (specimens N-C02RS and N-C24S) or near the shear key (specimens H-C02R and N-C02).

3.2. Bending-deformation amplitude and buckling-half-wave length

After completion of the test, each specimen was dissected to observe the deformation of the steel core and the surface of mortar. Figure 3.3 plots the distribution of peak minor-axis bending deformation of the steel core. Direct measurement was taken after removing the steel-and-mortar planks. The longitudinal distance, taken from the top end of the yielding segment, is taken as the abscissa. The figure indicates that the steel core buckled in a very high-mode after yielding in compression.

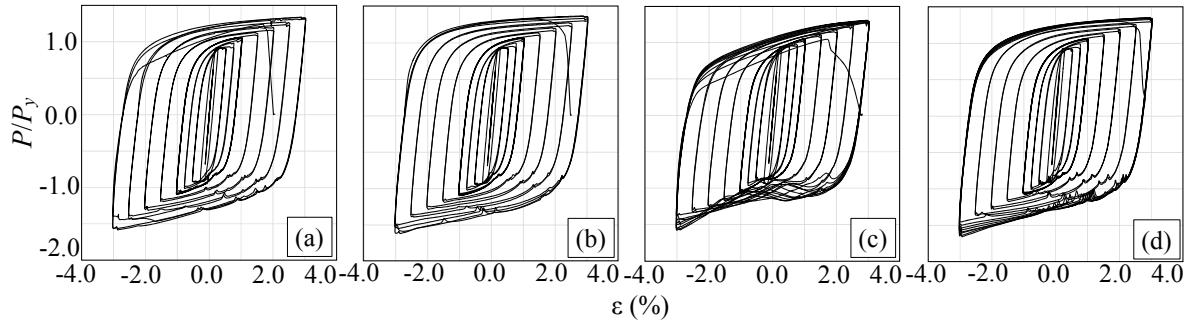

Figure 3.1 P/P_y – ε relationship : (a) N-C02RS ; (b) H-C02R ; (c) N-C24S ; (d) N-C02

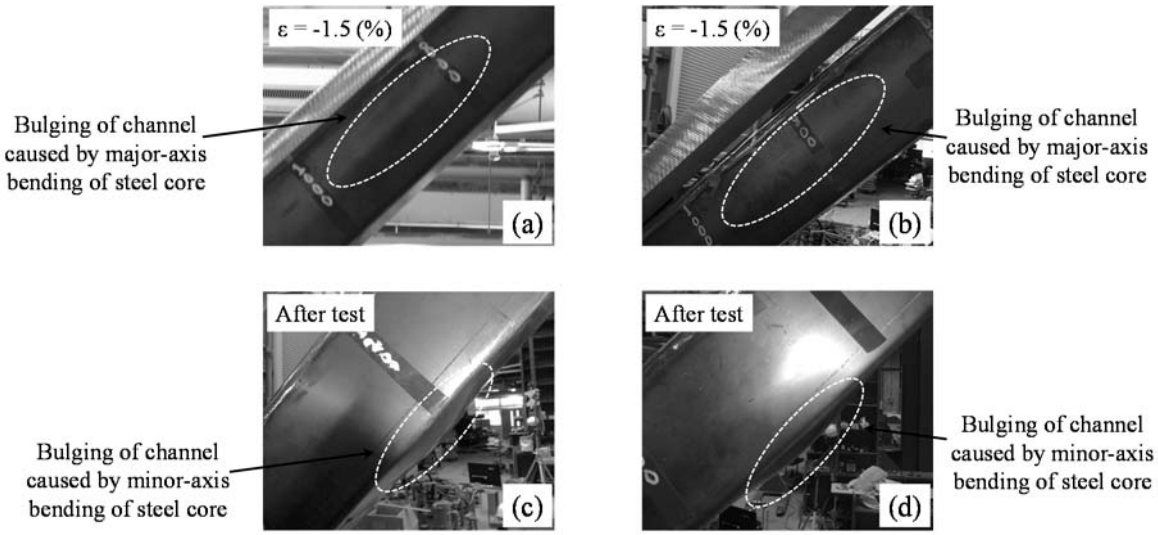

Figure 3.2 State of restraining system : (a) N-C24S and (b) N-C02 at ε = 1.5%;
(c) N-C02RS and (d) N-C24S at end of test

Table 3.1 Last half cycle and observations

Specimen	Last half cycle	Failure mode
N-C02RS	4th (+) 3.0%	Tensile fracture at lower end
H-C02R	5th (+) 3.0%	Tensile fracture at upper side near shear key
N-C24S	9th (+) 3.0%	Tensile fracture at lower end
N-C02	9th (+) 3.0%	Tensile fracture at lower side near shear key

3.2. Bending-deformation amplitude and buckling-half-wave length

After completion of the test, each specimen was dissected to observe the deformation of the steel core and the surface of mortar. Figure 3.3 plots the distribution of peak minor-axis bending deformation of the steel core. Direct measurement was taken after removing the steel-and-mortar planks. The longitudinal distance, taken from the top end of the yielding segment, is taken as the abscissa. The figure indicates that the steel core buckled in a very high-mode after yielding in compression. The deflection distributed symmetrically with respect to the shear key location (mid-length of the yielding segment). In specimens N-C02RS and N-C24S, the deformation amplitude was larger near the end of yielding segment. In specimens H-C02R and N-C02, the deformation amplitude was evenly distributed along the yielding segment.

Figure 3.4 plots the distribution of half-wave length of minor-axis bending deformation at the end of the test. The wave number, counted starting from the top end of the yielding segment, is taken as the abscissa. In specimens N-C02RS and N-C24S, the half wave length was shorter near the core projection and longer near the shear key. In specimens H-C02R and N-C02, the half-wave length was more uniform throughout yielding segment.

Figure 3.5 plots the distribution of peak major-axis bending deformation of the steel core at the end of the test. Compared to the minor-axis bending deformation shown in Figure 3.3, major-axis bending deformation occurred in a very low buckling mode. The deformation of specimen N-C24S was much larger than the other specimens. As previously discussed with Figure 3.2, the bulging of channel in specimens N-C24S and N-C02 was likely caused by major-axis bending deformation of the steel core. In specimen N-C24S, the steel core was given a larger clearance of C_s = 12 mm to deform before reaching the channel, while specimen N-C02 was given the same clearance as the other two specimens, C_s = 1 mm. The absence of round bar in specimen N-C02 led to bulging of the channel but did not affect major-axis bending deformation of the steel core.

Figure 3.6 illustrates the mortar condition at the end of the test. In specimens H-C02R and N-C02, the mortar was damage free aside from localized cracks. On the other hand, in specimens N-C02RS and N-C24S, the mortar spalled near the core projection and near the shear key. Specimens N-C02RS and N-C24S used a

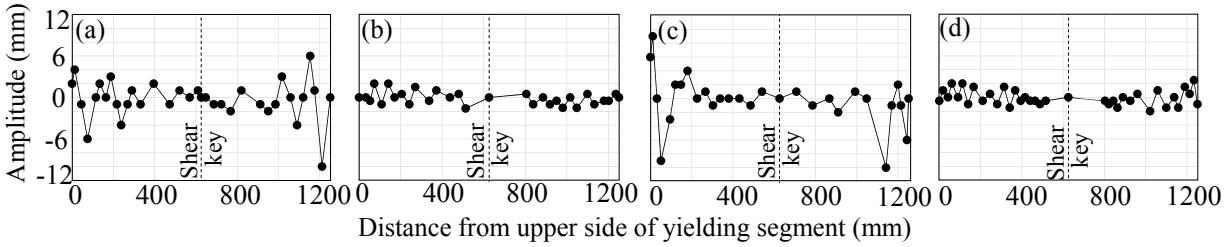

Figure 3.3 Minor-axis bending deformation: (a) N-C02RS ; (b) H-C02R ; (c) N-C24S ; (d) N-C02

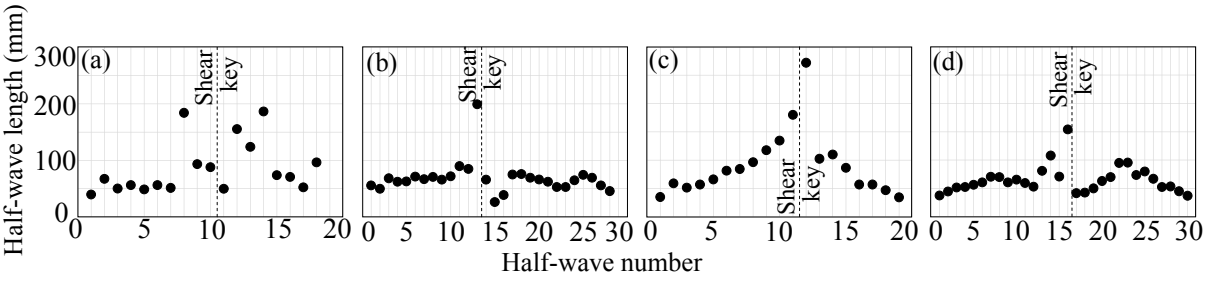

Figure 3.4 Half-wave length : (a) N-C02RS ; (b) H-C02R ; (c) N-C24S ; (d) N-C02

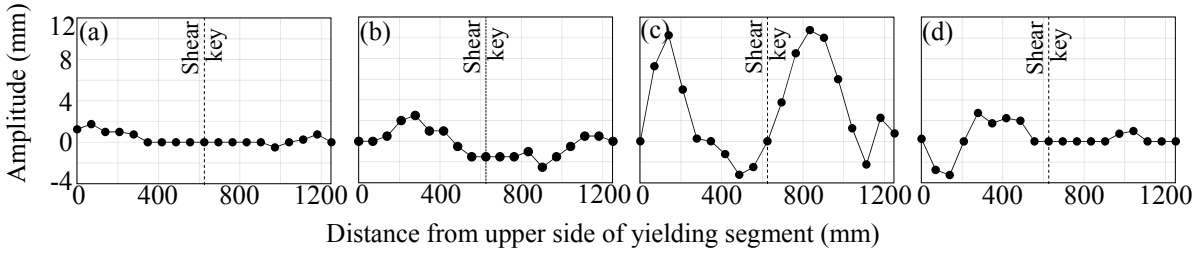

Figure 3.5 Major-axis bending deformation: (a) N-C02RS ; (b) H-C02R ; (c) N-C24S ; (d) N-C02

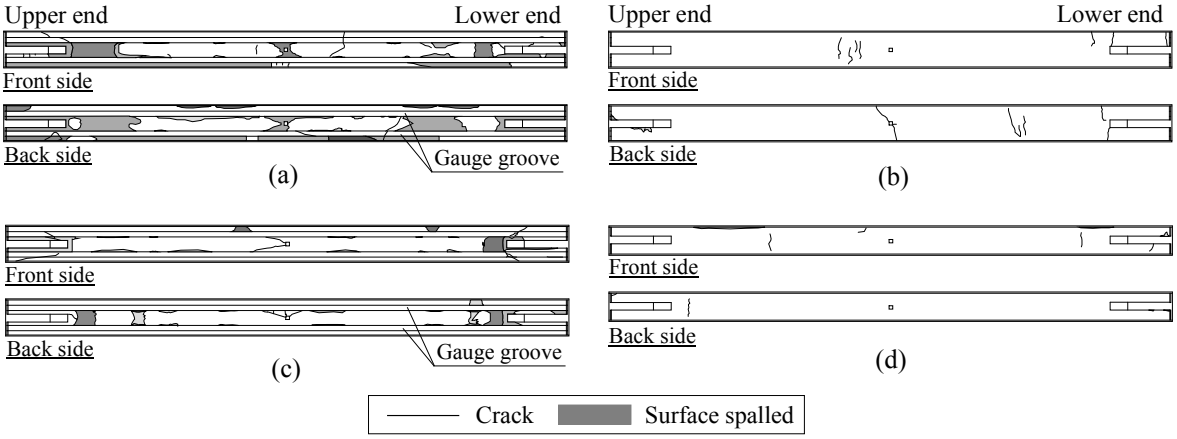

Figure 3.6 Observed damage in mortar : (a) N-C02RS ; (b) H-C02R ; (c) N-C24S ; (d) N-C02

standard shape steel-and-mortar plank, while specimen H-C02R used high-strength steel for the channel and specimen N-C02 used a deeper plank that could have resulted in extra strength and stiffness of the buckling-restraining system. The extra strength and stiffness may have reduced the damage of the mortar.

3.3. Cumulative plastic strain energy ratio

Figure 3.7 plots the relationship between the normalized dissipated energy, ω, obtained by dividing the dissipated strain energy by the product of P_y and elastic limit deformation, δ_y, and the cumulative strain, $\Sigma|\varepsilon|$. Each plot ends where the steel core fractured. The increase rate of ω with respect to $\Sigma|\varepsilon|$ was lower for specimens N-C24S than for the other three specimens. The lower rate is attributed to decrease in strength associated with major-axis bending deformation: specimen N-C24S deformed significantly in major-axis bending from strain amplitude of 1.0%, while such deformation was minimal in the other specimens.

Iwata and Murai (2006) and Iizuka et al. (2014), proposed the following formula to predict the energy dissipation capacity of BRBs, ω_{last}, in terms of P_E/P_y.

$$\omega_{last} = 150\, P_E/P_y \quad (P_E/P_y < 6) \tag{1a}$$

$$\omega_{last} = 900 \quad (P_E/P_y \geqq 6) \tag{1b}$$

The formula predicts the lower bound energy dissipation capacity for BRBs designed mainly with P_E/P_y = 3.0 to 4.5. For the BRBs in this project, all designed with P_E/P_y = 6, the formula predicts ω_{last} = 900. Figure 3.7 shows that specimens N-C24S and N-C02 exceeded the prediction while specimens N-C02RS and H-C02R failed to reach this prediction. This result is counterintuitive because the two specimens that controlled major-axis bending deformation underperformed specimen N-C24S that did not controlled major-axis bending deformation. The reason why specimens N-C02RS and H-C02R failed to reach the prediction is a subject for further research.

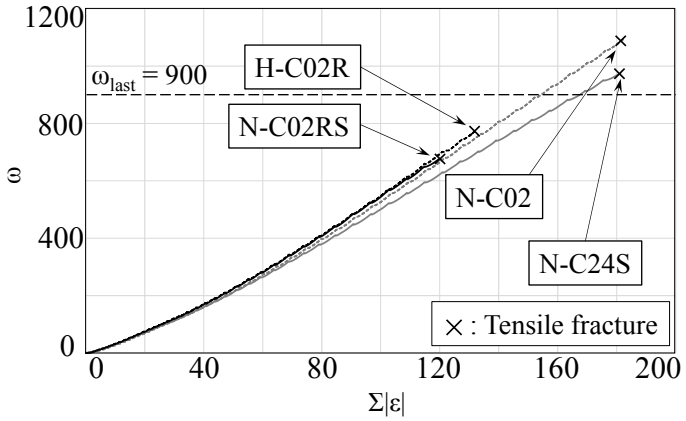

Figure 3.7 ω－Σ|ε| relationship

3.4. Buckling-mode number in minor-axis bending

Figure 3.8 shows the relationship between the strength increase ratio in compression, P_c/P_y and buckling-mode number, M, in minor-axis bending. The dark and gray filled circles indicate the buckling-mode number evaluated based on strain gauge measurements during the test; and the open circles indicate the buckling-mode number based on direct measurement after the test. The solid line indicates the relationship proposed by Midorikawa et al. (2010) written in Formula (3) and (4) below.

$$M = \frac{\lambda_w}{\pi}\sqrt{\frac{\sigma_y (P_c/P_y)}{E}} \quad (P_c/P_y < 1) \tag{3}$$

$$M = \frac{\lambda_w}{\pi}\sqrt{\frac{\sigma_y}{E}}\left(\sqrt{\frac{(P_c/P_y)-1}{E_r/E}}+1\right) \quad (P_c/P_y \geqq 1) \tag{4}$$

In the above equations, E is the Young's modulus of the steel core, and E_r is computed as follows.

$$E_r = \frac{4EE_t}{\left(\sqrt{E_t}+\sqrt{E}\right)^2} \tag{5}$$

The tangent modulus, E_t, was set equal to $0.03E$. According to Figure 3.8, Formulas (3) and (4) matches specimens N-C02RS and N-C24S, but does not match specimens H-C02R and N-C02. It is suspected that the larger than ordinary strength and stiffness of the buckling-restraining system, mentioned in Section 3.3, caused the steel core to buckle in a higher mode than observations in earlier tests that formed the basis of the formulas.

3.5. Overstrength ratio

Figure 3.9 shows relationship between the overstrength in compression, P_c/P_y and cumulative average strain, $\Sigma|\varepsilon|$. Figure 3.9 shows little difference among four specimens up to $\Sigma|\varepsilon| = 100$. Towards the end of the test, P_c/P_y decreased in a different rate among four specimens. Midorikawa et al. (2012) observed that increase in

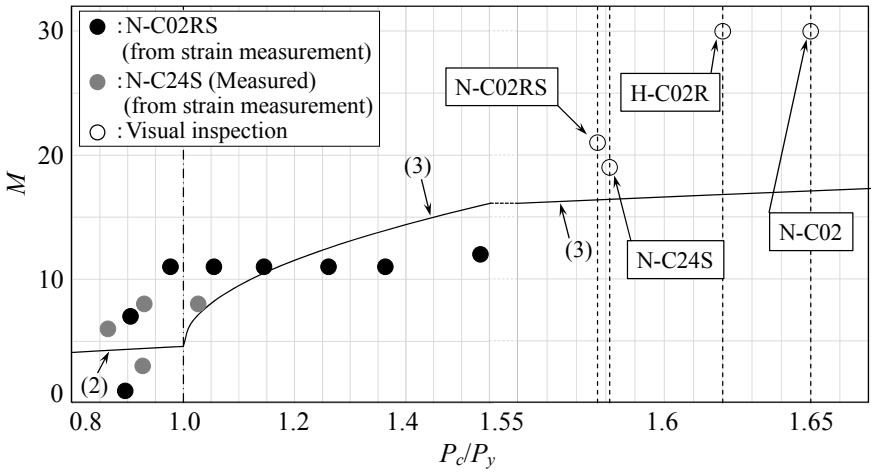

Figure 3.8 $P_c/P_y - M$ relationship

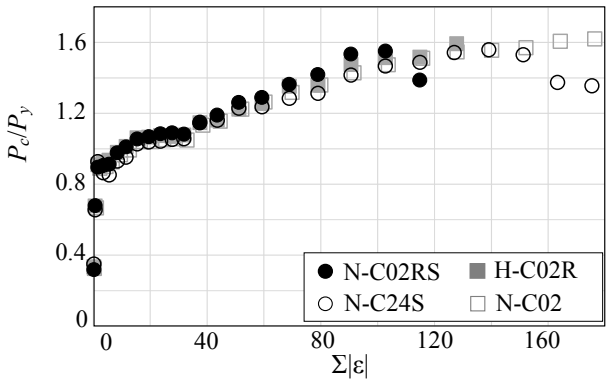

Figure 3.9 $\Sigma|\varepsilon| - P_c/P_y$ relationship

P_c/P_y is caused by contact between the steel core and mortar, through which a portion of the compressive force is transferred from the steel core to the buckling restraining system. It is natural to believe that the contact occurred at the peak deformation points shown in Figure 3.3. For specimens N-C02RS and H-C02R, concentration of contact points near the ends of the yielding segment (see Figure 3.4) may have been the cause of damage to the mortar (Figure 3.6), which led to deformation concentration (Figure 3.3), and ultimately, failure at the end of the yielding segment. For specimens H-C02R and N-C02, the contact points distributed evenly. The deformation concentration may explain why P_c/P_y decreased in a higher rate in specimens N-C02RS and H-C02R.

4. CONCLUSIONS

Four full-scale BRB specimens were subjected to cyclic loading to examine the relationship between steel core deformation and the cyclic loading performance of BRBs. The main findings are listed below:

1) Major-axis bending deformation of the steel core is a concern for BRBs using steel-and-mortar planks because a gap is left between the steel core and steel casing that is not filled with mortar. However, the deformation may be controlled effectively by: (a) filling the gap with a round bar; or (b) leaving the gap (dimension C_s in Figure 2.2) small.
2) Control of major-axis bending deformation leads to more stable hysteretic behavior. However, interestingly, in terms of energy dissipation, strict control of major-axis bending deformation may not be beneficial.
3) The performance of the BRB is controlled primarily by bracing of minor-axis bending deformation. A stiff and strong bracing system can increase the buckling mode number, and thereby increase the overstrength ratio in compression, but on the other hand, evenly distribute the high-mode buckling deformation, and thereby avoid deformation concentration in the steel core.

ACKNOWLEDGEMENT

The authors would like to acknowledge Koyano, K., Research associate, Kanagawa Univ., M. Eng., and T. Tanaka, former graduate student of Kanagawa Univ., B. Eng. for excellent assistance.

REFERENCES

1. Iwata, M. and Murai, M. (2006). Buckling-Restrained Brace Using Steel Mortar Planks; performance evaluation as a hysteretic damper. *Earthquake Engineering and structural Dynamics* **35:14**, 1807-1826
2. Hishida, S., Ohura, T., Midorikawa, M., Iwata, M., Okazaki, T., and Asari, T. (2015). Experimental Study on Buckling-Restrained Braces Using Steel-and-Mortar Planks -Effect of Steel Shear Key Location on the Performance and Evaluation of Buckling Deformation-. *Journal of Structural Engineering*, AIJ **61B**, 141-149 (in Japanese)
3. Midorikawa, M., Wakayama, T., Asari, T., and Iwata, M. (2014a). Experimental Study on Buckling-Restrained Braces Using Steel Mortar Planks -Evaluation of Estimation Method of Compressive-to-Tensile Strength Ratio Considering the Distribution of Friction Forces-. *Journal of Structural Engineering*, AIJ **60B**, 307-315 (in Japanese)
4. Midorikawa, M., Iwata, M., Wakayama, T., Iizuka, R., Okazaki, T. and Asari, T. (2014b), Buckling-mode Number and Compressive-to-tensile Strength Ratio of Buckling-restrained Braces, *Proceedings of the 10th U.S. National Conference on Earthquake Engineering*, Paper No. 660, Anchorage, Alaska, U.S.A.
5. Midorikawa, M., Asari, T., Iwata, M., Murai, M. and Tanaka, Y. (2012), Cyclic Behaviour of Buckling-restrained Braces Using Steel Mortar Planks; Buckling Mode Number and Strength Ratio, *Proceedings of the 15th World Conference on Earthquake Engineering*, Paper ID: 0572, Lisbon, Portugal
6. Midorikawa, M., Sasaki, D., Asari, T., Murai, M., and Iwata, M. (2010). Experimental Study on Buckling-Restrained Braces Using Steel Mortar Planks -Effects of the Clearance between Core Plate and Restraining Member on Compressive Strength and Estimation of the Number of Buckling Mode Related to Compressive Strength-. *Journal of Structural Construction Engineering*, AIJ **75:653**, 1361-1368 (in Japanese)
7. Iizuka, R., Koyano, K., Midorikawa, M., and Iwata, M. (2014). Study on Buckling-Restrained Braces Having Large Cumulative Plastic Strain Energy Ratio. *Journal of Structural Construction Engineering*, AIJ **79:701**, 1015-1023 (in Japanese)